

Article

Heat Transfer and Entropy Generation for Mixed Convection of Al_2O_3 –Water Nanofluid in a Lid-Driven Square Cavity with a Concentric Square Blockage

M. Özgün Korukçu 

Department of Mechanical Engineering, University of Bursa Uludag, Gorukle, 16059 Bursa, Turkey; ozkorukcu@uludag.edu.tr

Abstract: The present numerical investigation is focused on analyzing the characteristics of steady laminar mixed convection flow in a lid-driven square cavity, specifically considering the utilization of Al_2O_3 –water nanofluid. The Al_2O_3 –water nanofluid is assumed to be Newtonian and incompressible. Within the cavity, a square blockage is positioned at its center, which is subjected to isothermal heating. The blockage ratio of the square is $B = 1/4$, and the Grashof number is $Gr = 100$. The walls of the cavity are maintained at a constant temperature, T_c , while the square blockage remains at a constant temperature, T_h . The primary objective of this study is to investigate the flow and heat transfer mechanisms, as well as the entropy generation within the cavity. This investigation is conducted for a range of Richardson numbers ($0.01 \leq Ri \leq 100$) and volume fractions of the nanofluid ($0 \leq \phi \leq 0.05$). Several parameters are obtained and analyzed, including streamlines, isotherms, velocity variations on the vertical and horizontal midplanes, local Nusselt number variations on the surfaces of the square blockage, the average Nusselt number on the square blockage, and the total dimensionless entropy generation of the system. The results of the investigation revealed that both the average Nusselt number on the square blockage and the total dimensionless entropy generation of the system exhibit an increasing trend with an increasing volume fraction of the nanofluid and a decreasing Richardson number. Furthermore, correlations for the average Nusselt number and the total dimensionless entropy generation with the Richardson number, and the nanofluid volume fraction are derived.



Citation: Korukçu, M.Ö. Heat Transfer and Entropy Generation for Mixed Convection of Al_2O_3 –Water Nanofluid in a Lid-Driven Square Cavity with a Concentric Square Blockage. *Processes* **2024**, *12*, 1079. <https://doi.org/10.3390/pr12061079>

Academic Editors: David Cabaleiro and Jacek Fal

Received: 15 April 2024

Revised: 10 May 2024

Accepted: 21 May 2024

Published: 24 May 2024



Copyright: © 2024 by the author. Licensee MDPI, Basel, Switzerland. This article is an open access article distributed under the terms and conditions of the Creative Commons Attribution (CC BY) license (<https://creativecommons.org/licenses/by/4.0/>).

Keywords: heat transfer; entropy generation; lid-driven cavity; mixed convection; nanofluid

1. Introduction

The lid-driven cavity flow problem holds substantial importance in both engineering and applied sciences. Primarily, it serves as a fundamental problem for validating code solutions for Navier–Stokes equations [1,2]. Additionally, it is employed in various applications, including the cooling of electronic equipment, nuclear reactors, solar energy collection, heat exchangers, and crystal growth [3]. The forced convection is induced by the movement of the cavity’s lid, while the temperature disparity within the cavity gives rise to natural convection, resulting in the formation of a combined convection flow [4]. The mixed convection flow in a lid-driven cavity has been the subject of numerous research studies conducted by scholars. The cavity can be in different shapes such as waves, with fins, blockage inside the cavity, porous media, or inclined. To enhance the heat transfer, nanofluids can be used as Al_3O_2 , Cu, CuO, TiO_2 , SiO_2 , Ag, and Fe_3O_4 [5]. Iwatsu et al. [6] conducted a study on the mixed convection flow within a square cavity, where the sidewalls were adiabatic while the top and bottom walls were maintained at varying temperatures. The study focused on analyzing the velocity and temperature profiles of the mixed convection flow under different Grashof and Reynolds (Gr/Re^2) numbers. The investigation carried out by Malleswaran and Sivasankan [7] focused on the analysis of magneto-hydrodynamics mixed convection in a lid-driven cavity equipped with corner heaters. The researchers aimed to

explore the influence of different heater lengths on the heat transfer rate. To regulate the flow and temperature within the lid-driven enclosure, the placement of an object inside the cavity was employed as a control mechanism. They reported that the magnetic field affects the average heat transfer rate more on vertical heaters than on horizontal heaters. In their study, Oztop et al. [8] examined the phenomenon of mixed convection in a square cavity with a circular body. The cavity was driven by a lid, with the left and right walls being heated. However, the left wall was maintained at a higher temperature compared to the right wall. The top and bottom walls of the cavity were adiabatic. The circular body within the cavity could be adiabatic, isothermal, or conductive. The researchers explored various scenarios by considering different values of the Richardson number, the orientation of the lid, and the diameter of the circular body. Through their investigation, they found that the orientation of the moving lid had the most significant impact on the flow field and temperature distribution within the cavity. Another remarkable result was the thermal conductivity becomes insignificant for small values of the diameter of the circular body. In their study, Khanafer and Aithal [9] employed a finite element method to examine the flow and heat transfer properties of laminar mixed convection in a square lid-driven cavity. Their findings revealed that the Nusselt number exhibited an upward trend when a built-in cylinder was present within the cavity, as opposed to an empty cavity. Additionally, they explored the influence of the Richardson number, non-dimensional circle diameter, and the positioning of the circular cylinder body on the Nusselt number. For dominant mixed convection, the average Nusselt number increases with an increase in the radius of the cylinder for various Richardson numbers. Zheng et al. [10] conducted an additional investigation on the mixed convection flow within a lid-driven cavity, taking into account the existence of a circular cylinder. The study focused on examining the impact of the cylinder's position and the changes in Reynolds number while maintaining a constant Grashof number. The researchers reached a significant conclusion that the location of the cylinder has a notable influence on the fluid flow and heat transfer properties. Islam et al. [11] studied numerical simulations of mixed convection in a lid-driven cavity with an isothermally heated square. For a fixed Reynolds number of $Re = 100$ and Prandtl number of $Pr = 0.71$ effects of the Grashof number, square eccentricity, and blockage ratio of the square on heat transfer and flow characteristics were investigated. The average Nusselt number values of the square block for different positions of the square and the blockage ratio were obtained. The highest average Nusselt number values were obtained for the blockage near the top wall. The impact of the position of square cylinders on the average Nusselt number values was examined in a study conducted by Morshed et al. [12]. The study focused on the laminar mixed convection flow occurring in a lid-driven cavity, where two square cylinders were isothermally heated. While the researchers altered the position of the square cylinders and adjusted the Reynolds number, they kept the Prandtl number and Grashof number constant. The results demonstrated a significant influence of the square cylinder location on the average Nusselt number values and the separation distance between the two blockages had a large effect on the total average Nusselt number. Gangawane [13] conducted a study on the mixed convection heat transfer characteristics in a lid-driven cavity with the presence of a triangular block. The research focused on examining the heat and flow characteristics when a constant heat flux was applied to the triangular block, considering various blockage ratios, Reynolds numbers, Grashof numbers, and Prandtl numbers. The investigation resulted in the determination of both local and average Nusselt number values on the triangular block. It was observed that an increase in Reynolds number enhances the heat transfer rate only up to $Re = 180$ – 220 ; later, a decrease of heat transfer rate is observed.

The application of nanofluid leads to an improvement in the rate of heat transfer. According to Choi and Eastman [14], the addition of nanoparticles to the base fluid enhances its thermal conductivity. In their study, Xuan and Li [15] proposed a technique for creating nanofluids and found that the thermal conductivity of these fluids is influenced by various factors such as the volume fraction, shape, dimensions, and properties

of the nanoparticles. In their study, Khanafer et al. [16] investigated the enhancement of buoyancy-driven heat transfer in a two-dimensional enclosure using nanofluids. To solve the transport equations, they employed the finite volume method. The researchers explored the influence of the Grashof number and the volume fractions of the nanofluid, and subsequently derived correlations for the Nusselt numbers. Abu-Nada and Chamkha [17] conducted a study where they provided numerical solutions for the mixed-convection flow in an inclined square cavity driven by a lid, using water–Al₂O₃ nanofluid. The non-dimensional vorticity stream-function equations were solved using a second-order-accurate finite volume method. The study examined the variations of the Nusselt number with the Richardson number, inclination angle, and volume fraction of the nanofluid. The presence of nanoparticles increased heat transfer, and this was accentuated by the inclination of the enclosure at moderate and large Richardson numbers. In their investigation, Mansour et al. [18] explored the numerical simulation of mixed convection flows in a square cavity with a lid-driven motion. The cavity was partially heated from below and filled with a nanofluid. To solve the dimensionless governing equations, the researchers employed a finite difference method. Specifically, they focused on water-based nanofluids containing Cu, Ag, Al₂O₃, and TiO₂ particles. The study aimed to analyze the impact of various factors, including the Reynolds number, solid volume fraction, heat source length, and heat source location, on the characteristics of heat transfer and fluid flow. They reported that when the heat source length was increased, heat transfer was decreased, and placing the heat source at the left half of the bottom wall gave large rates of heat transfer. In their study, Talebi et al. [19] conducted numerical simulations to investigate the mixed convection phenomenon in a square lid-driven cavity using Cu–water nanofluid. The researchers analyzed the hydrodynamics and thermal properties of the flow under various conditions, including different Rayleigh numbers, Reynolds numbers, and solid volume fractions of the nanofluid. The authors found that at the fixed Reynolds number, the solid concentration affects the flow pattern and thermal behavior, particularly for a higher Rayleigh number. Chamkha and Abu-Nada [20] examined the impact of different viscosity models on the mixed convection flow within single and double-lid-driven cavities using water–Al₂O₃ nanofluid. Specifically, they compared the Brinkman model with the Pak and Cho correlation. The researchers discovered that when the nanofluid was modeled using Pak and Cho’s approach, there was a decrease in the average Nusselt number for the single lid-driven case. Mojumder et al. [21] investigated the impact of Reynolds and Grashof numbers on mixed convection within a lid-driven T-shaped cavity containing water–Al₂O₃ nanofluid. The study revealed that the Grashof, Reynolds, Richardson, and volume fractions of the nanoparticles play a crucial role in determining the heat transfer characteristics. Additionally, the researchers provided visual representations of the flow through isotherm and streamlines and calculated the average Nusselt numbers for the heated moving wall. In their study, Kareem et al. [22] conducted an investigation on the mixed convection of nanofluids within a trapezoidal cavity driven by a lid. To solve the governing equations, they employed a finite volume method. The researchers utilized four different types of nanofluids, namely Al₂O₃, CuO, SiO₂, and TiO₂, mixed with water. They examined the impact of various factors such as the aspect ratio and inclination of the cavity, nanoparticle volume fraction, nanoparticle diameter, Reynolds number, and Richardson number on the heat transfer characteristics. Notably, the nanofluid containing SiO₂ exhibited higher Reynolds numbers compared to the other nanofluids. Numerical simulations were conducted by Taamneh and Bataineh [23] to investigate the mixed convection flow in a square lid-driven cavity that was filled with water–Al₂O₃ nanofluid. The study focused on analyzing the variations of streamlines, isotherms, and the average Nusselt number of the hot-moving lid. These variations were observed for different volume fractions of the nanofluid, Reynolds numbers, and Richardson numbers. The findings of the study were presented and discussed in detail. A study conducted by Astanina et al. [24] investigated the mixed convection of a water–Al₂O₃ nanofluid in a lid-driven cavity with two porous layers. The researchers employed the stream function and vorticity equations to solve the

flow field, while the Brinkman-extended Darcy model was utilized for the porous layers. The study focused on examining the impact of various factors, including the Richardson number, Darcy number, porous layer thickness, and volume fraction of the nanofluid, on the heat transfer characteristics. It was found that in the natural convection regime, an addition of nanoparticles leads to heat transfer enhancement, while for mixed convection and forced convection regimes, an increase in nanoparticle volume fraction leads to heat transfer reduction. Cho [25] conducted a study that examined the heat transfer and entropy generation of a mixed convection flow of Cu–water nanofluid in a lid-driven cavity with a wavy surface. The research aimed to determine the total entropy generation, Nusselt number, and Bejan numbers under different conditions, including Richardson numbers, the amplitude of the wavy surface, and the volume fraction of the nanofluid. An optimal heat transfer effect was obtained given an appropriate wavelength of the wavy surface depending on the Richardson numbers. In their research, Mehmood et al. [26] investigated the phenomenon of mixed convection within a lid-driven cavity filled with a water–Al₂O₃ nanofluid. The cavity contained a square object that was heated isothermally, and the study also considered the influence of a magnetic field. To solve the governing equations, the researchers employed the Galerkin finite element method. By varying the Reynolds number, Richardson number, Hartmann number, and Eckert number, they were able to obtain the average Nusselt number, entropy generation, and average temperature values. An increase in average temperature in the cavity has been noticed with an augmentation in Eckert number and magnetic field strength. The investigation carried out by Karbasifar et al. [27] involved numerical simulations of mixed convection in a lid-driven cavity filled with water–Al₂O₃ nanofluid. The cavity contained a hot elliptic cylinder, and the researchers examined the heat transfer characteristics under various conditions. Specifically, they studied the effects of Richardson numbers, volume fraction of the nanofluid, and inclination angles while maintaining a constant temperature difference. They concluded that the effect of changing the cavity angle on heat transfer and Nusselt number is much smaller than the Richardson number and volume fraction. Azizul et al. [4] utilized the finite element method to address the mixed convection flow occurring in a wavy heated cavity. The investigation focused on the inclusion of nanofluids and an inner solid block within the cavity. Various parameters, such as Reynolds number, Grashof number, volume fraction of nanoparticles, fraction of undulations, and blockage of the inner solid block, were considered to analyze the flow and heat transfer characteristics. According to the results, the size of the internal object minimizes the space inside the wavy cavity, and it was found that $D = 0.3$ is the perfect size located within the center of the cavity. Rajesh and Sheremet [28] performed numerical simulations to investigate the phenomenon of free convection in a square cavity with a lid-driven flow. The cavity was filled with a ternary hybrid nanofluid, specifically composed of Cu–CuO–Al₂O₃ and water. They showed that ternary nanofluids can be more effective compared to mono- and hybrid nanofluids.

The field of thermal engineering not only focuses on heat transfer analyses but also recognizes the crucial role played by entropy generation. Viscosity is another important parameter in fluid flow analyses [29]. The research conducted by Chamka et al. [30] involved numerical analyses of various electrical conductivity models for magneto-hydrodynamic mixed convection of nanofluids in a triangular cavity with a lid-driven flow. The finite element method was employed to carry out the simulations. The study aimed to explore the impact of Richardson and Hartman numbers on heat transfer and entropy generation. They stated that the magnetic field affected the behaviors of entropy generation rate versus solid particle volume fraction. Alshare et al. [31] conducted a study on the natural convection of Al₂O₃–water nanofluid in a lid-driven cavity with an elliptical shape and a wavy boundary heated from the bottom. The research focused on examining the impact of the ovoid's orientation at the center and the undulation number of the wave on both heat transfer and entropy generation. Heat transfer was responsible for entropy generation, while frictional and magnetic effects were marginal. Ishak et al. [32] conducted a study on a different mixed convection scenario involving Al₂O₃–water nanofluid. In their investigation, they focused

on evaluating the entropy generation of the mixed convection flow within a trapezoidal lid-driven cavity that contained a solid cylinder. The researchers determined that the size and position of the solid cylinder played a crucial role in influencing heat transfer properties and entropy generation. The maximum average Nusselt numbers were obtained for high radius values, where the average Nusselt number was increased by 30% when the radius was raised from 0 to 0.25. Laidoudi et al. [33] conducted a study where they examined a lid-driven cavity with a 3D elliptical obstacle. They used the Galerkin finite element method to analyze the effects of different factors, such as properties of Al_2O_3 -Cu-water nanofluid, Lorentz force, thermal buoyancy, and space porosity, on heat transfer and entropy generation. According to their results, increasing the value of Darcy and/or Reynolds number increases the average Nusselt of the obstacle and the magnetic field decreases the heat transfer rate. Maneengam et al. [34] also investigated heat transfer, flow mechanism, and entropy generation in a corrugated porous cavity filled with a hybrid nanofluid Fe_3O_4 -MWCNT-water. They specifically focused on these phenomena in the presence of a magnetic field. The change in the shape of the obstacle from the elliptical to triangular raised the value of Nusselt number at a rate of 15.54% for $Ha = 0$, $N = 8$, and $Gr = 10,000$. Maneengam et al. [35] conducted another study where they explored the generation of entropy in a porous cavity driven by a lid. The cavity was filled with different obstacles and subjected to buoyancy and Lorentz forces. The researchers modified the shapes of the obstacles, including elliptical, square, triangular, and circular forms, while the lower wall of the cavity was designed with wave patterns. Increasing the Hartman and decreasing the Reynolds numbers drops both the irreversibility and the heat transfer rate. Taghizadeh and Adaditaheri [36] performed computational investigations on the heat transfer and entropy generation characteristics of laminar mixed convection within an inclined lid-driven enclosure containing a circular porous cylinder. They stated that the effect of the inclination angle on the heat transfer and entropy generation inside the enclosure is more noticeable at high Richardson numbers. Zeghibid and Bessaih [37] conducted a study on the mixed convection and entropy generation in a square cavity using nanofluids. The researchers filled the cavity with water-Cu-Ag- Al_2O_3 and TiO_2 nanofluids and introduced two heat sources. The investigation focused on examining the impact of the Richardson number, Reynolds number, and solid volume fraction of nanofluids on heat transfer and entropy generation. They found that entropy generation decreased with increasing solid volume fraction, Rayleigh numbers, and Reynolds numbers.

This study focuses on analyzing the laminar mixed convection flow in a square lid-driven cavity. The cavity contains a square blockage at its center and is filled with Al_2O_3 -water nanofluid. The Grashof number is kept constant while the Reynolds number is varied, and different volume fractions of Al_2O_3 nanoparticles are considered. The study visually presents the streamlines and isotherms of the flow to understand the fluid behavior. It also calculates the local and average Nusselt numbers on the surfaces of the square blockage to analyze the heat transfer characteristics. Additionally, the total dimensionless entropy generation of the system is determined to gain insights into the overall thermodynamic behavior. To establish relationships between the average Nusselt number and the total dimensionless entropy generation, correlations are derived. These correlations take into account different values of the Richardson number and the volume fraction of the nanofluid. By examining these correlations, it becomes possible to predict the heat transfer and entropy generation characteristics of the system under different conditions.

2. Materials and Methods

2.1. Problem Description

The current investigation focuses on the analysis of a mixed convection problem occurring in a lid-driven cavity that is filled with Al_2O_3 -water nanofluid. The cavity contains a square blockage positioned at its center, as depicted in Figure 1. Both the height ($H = 1$ m) and length ($L = 1$ m) of the cavity are identical, and the square blockage has a dimension of $B = D/H$, where D represents the length of the blockage ($B = H/4$). The

walls of the cavity are maintained at a cold temperature (T_c), while the walls of the square blockage are kept at a hot temperature (T_h). The right, left, and bottom walls of the cavity remain stationary, while the top wall moves towards the right with a velocity of U_{lid} . Additionally, a negative gravitational acceleration is considered in the y -direction within the cavity.

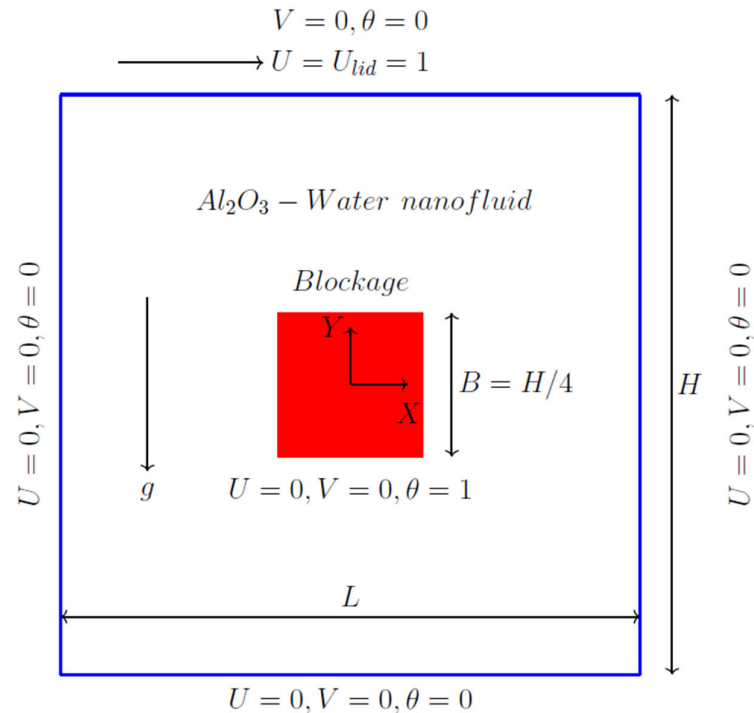


Figure 1. Physical model of the problem.

2.2. Governing Equations

The Navier–Stokes and energy equations are employed to solve the steady, two-dimensional, incompressible laminar mixed convection flow of Al_2O_3 –water nanofluid. The thermophysical properties of the nanofluid remain constant throughout the analysis, except for the buoyancy term, which is approximated using the Boussinesq approximation. Table 1 provides the thermophysical properties of both water and Al_2O_3 .

Table 1. Thermophysical properties of water and Al_2O_3 at 293 K [17].

Thermophysical Property	Water	Al_2O_3
C_p (J/kgK)	4179	765
ρ (kg/m^3)	997.1	3970
k (W/mK)	0.613	25
$\beta \times 10^5$ (1/K)	21	0.85
μ (Ns/m^2)	0.001003	-

The density, heat capacitance, and thermal expansion coefficient of the nanofluid can be determined using the physical mixture rule, as stated in [16].

$$\rho_{nf} = (1 - \phi)\rho_f + \phi\rho_{sp} \quad (1)$$

$$(\rho C_p)_{nf} = (1 - \phi)(\rho C_p)_f + \phi(\rho C_p)_{sp} \quad (2)$$

$$(\rho\beta)_{nf} = (1 - \phi)(\rho\beta)_f + \phi(\rho\beta)_{sp} \quad (3)$$

where f and sp represent the fluid and solid, respectively. The solid volume fraction is ϕ .

The thermal conductivity of the nanofluid can be calculated by Maxwell–Garnett’s model [38]:

$$k_{nf} = k_f \left[\frac{(k_{sp} + 2k_f) - 2\phi(k_f - k_{sp})}{(k_{sp} + 2k_f) + \phi(k_f - k_{sp})} \right] \quad (4)$$

Nanofluid viscosity is expressed by using the Brinkman relation [39]:

$$\mu_{nf} = \mu_f(1 - \phi)^{-2.5} \quad (5)$$

The continuity, momentum, and energy equations in a 2D Cartesian coordinate system for Newtonian incompressible fluid are as follows [18]:

$$\frac{\partial u}{\partial x} + \frac{\partial v}{\partial y} = 0 \quad (6)$$

$$\rho_{nf} \left(u \frac{\partial u}{\partial x} + v \frac{\partial u}{\partial y} \right) = -\frac{\partial p}{\partial x} + \mu_{nf} \left(\frac{\partial^2 u}{\partial x^2} + \frac{\partial^2 u}{\partial y^2} \right) \quad (7)$$

$$\rho_{nf} \left(u \frac{\partial v}{\partial x} + v \frac{\partial v}{\partial y} \right) = -\frac{\partial p}{\partial y} + \mu_{nf} \left(\frac{\partial^2 v}{\partial x^2} + \frac{\partial^2 v}{\partial y^2} \right) + (\rho\beta)_{nf} g(T - T_c) \quad (8)$$

$$(\rho C_p)_{nf} \left(u \frac{\partial T}{\partial x} + v \frac{\partial T}{\partial y} \right) = k_{nf} \left(\frac{\partial^2 T}{\partial x^2} + \frac{\partial^2 T}{\partial y^2} \right) \quad (9)$$

Non-dimensional continuity, momentum, and energy equations can be written as follows [23]:

$$\frac{\partial U}{\partial X} + \frac{\partial V}{\partial Y} = 0 \quad (10)$$

$$U \frac{\partial U}{\partial X} + V \frac{\partial U}{\partial Y} = -\frac{\partial P}{\partial X} + \frac{\mu_{nf}}{\rho_{nf} \nu_f} \frac{1}{Re} \left(\frac{\partial^2 U}{\partial X^2} + \frac{\partial^2 U}{\partial Y^2} \right) \quad (11)$$

$$U \frac{\partial V}{\partial X} + V \frac{\partial V}{\partial Y} = -\frac{\partial P}{\partial Y} + \frac{\mu_{nf}}{\rho_{nf} \nu_f} \frac{1}{Re} \left(\frac{\partial^2 V}{\partial X^2} + \frac{\partial^2 V}{\partial Y^2} \right) + \frac{(\rho\beta)_{nf}}{\rho_{nf} \beta_f} Ri\theta \quad (12)$$

$$U \frac{\partial \theta}{\partial X} + V \frac{\partial \theta}{\partial Y} = \frac{\alpha_{nf}}{\alpha_f} \frac{1}{RePr} \left(\frac{\partial^2 \theta}{\partial X^2} + \frac{\partial^2 \theta}{\partial Y^2} \right) \quad (13)$$

Non-dimensional parameters are written as follows:

$$\begin{aligned} X &= \frac{x}{H} & Y &= \frac{y}{H} & U &= \frac{u}{U_{lid}} & V &= \frac{v}{U_{lid}} & P &= \frac{p}{\rho_{nf} U_{lid}^2} \\ \theta &= \frac{(T-T_c)}{(T_h-T_c)} & Re &= \frac{\rho_f U_{lid} H}{\mu_f} & Pr &= \frac{(\mu C_p)_f}{k_f} & \alpha &= \frac{k_{nf}}{(\rho C_p)_{nf}} & Ri &= \frac{Gr}{Re^2} \\ Nu &= -\frac{k_{nf}}{k_f} \frac{\partial \theta}{\partial n} & Gr &= \frac{g \rho_f^2 \beta_f (T_h - T_c) H^3}{\mu_f^2} \end{aligned}$$

where Re is the Reynolds number, Pr is the Prandtl number, Gr is the Grashof number, Ri is the Richardson number, and Nu is the Nusselt number. The average Nusselt number on the square blockage can be calculated by integrating the local Nusselt number on the surfaces and dividing it by the total length of the surfaces.

The local entropy generation due to heat transfer and fluid flow can be found as follows [37]:

$$s_{gen} = \frac{\kappa_{nf}}{T_0^2} \left[\left(\frac{\partial T}{\partial x} \right)^2 + \left(\frac{\partial T}{\partial y} \right)^2 \right] + \frac{\mu_{nf}}{T_0} \left\{ 2 \left(\frac{\partial u}{\partial x} \right)^2 + 2 \left(\frac{\partial v}{\partial y} \right)^2 + \left[\left(\frac{\partial u}{\partial y} \right) + \left(\frac{\partial v}{\partial x} \right) \right]^2 \right\} \quad (14)$$

Dimensionless entropy generation or entropy generation number is calculated as follows:

$$S_{gen} = \frac{\kappa_{nf}}{\kappa_f} \left[\left(\frac{\partial \theta}{\partial X} \right)^2 + \left(\frac{\partial \theta}{\partial Y} \right)^2 \right] + \frac{\mu_{nf}}{\mu_f} N_\mu \left\{ 2 \left(\frac{\partial U}{\partial X} \right)^2 + 2 \left(\frac{\partial V}{\partial Y} \right)^2 + \left[\left(\frac{\partial U}{\partial Y} \right) + \left(\frac{\partial V}{\partial X} \right) \right]^2 \right\} \quad (15)$$

where N_μ is the irreversibility distribution ratio:

$$N_\mu = \frac{\mu_f T_0}{k_f} \left(\frac{\alpha_f}{L \Delta T} \right)^2 \quad (16)$$

$$T_0 = \frac{T_h + T_c}{2} \quad \Delta T = T_h + T_c$$

The total dimensionless entropy generation can be found with the integration of Equation (13).

$$S_{total} = \int S_{gen} dV \quad (17)$$

2.3. Boundary Conditions

The dimensionless boundary conditions of the problem are as follows:

1. On the top wall: $U = 1$ $V = \theta = 0$
2. On the left wall: $U = V = \theta = 0$
3. On the right wall: $U = V = \theta = 0$
4. On the bottom wall: $U = V = \theta = 0$
5. On the square blockage: $U = V = 0$ $\theta = 1$

2.4. Numerical Method

The solutions to the continuity, momentum, and energy equations are obtained using ANSYS-FLUENT 18.2, a solver based on the finite volume method. The pressure–velocity coupling is resolved using the SIMPLE algorithm. A second-order scheme is employed for mixed convection, while the momentum equations utilize the second-order upwind scheme. The energy equations, on the other hand, are solved using the first-order upwind scheme. To achieve convergence, a criterion of 10^{-6} is set for the continuity, momentum, and energy equations.

The structured grid of the problem is depicted in Figure 2. A finer grid is employed in the vicinity of the moving lid and square blockage surfaces. To ensure the reliability of the results, a grid independence study is conducted using pure water ($\phi = 0$) at $Gr = 100$ and $Ri = 0.1$. The average Nusselt number on the square blockage surfaces is found to be almost identical for grids with 72,960 and 80,800 nodes, as indicated in Table 2. Therefore, the numerical results in this study are obtained using a grid consisting of 80,800 nodes and a constant Grashof number of $Gr = 100$.

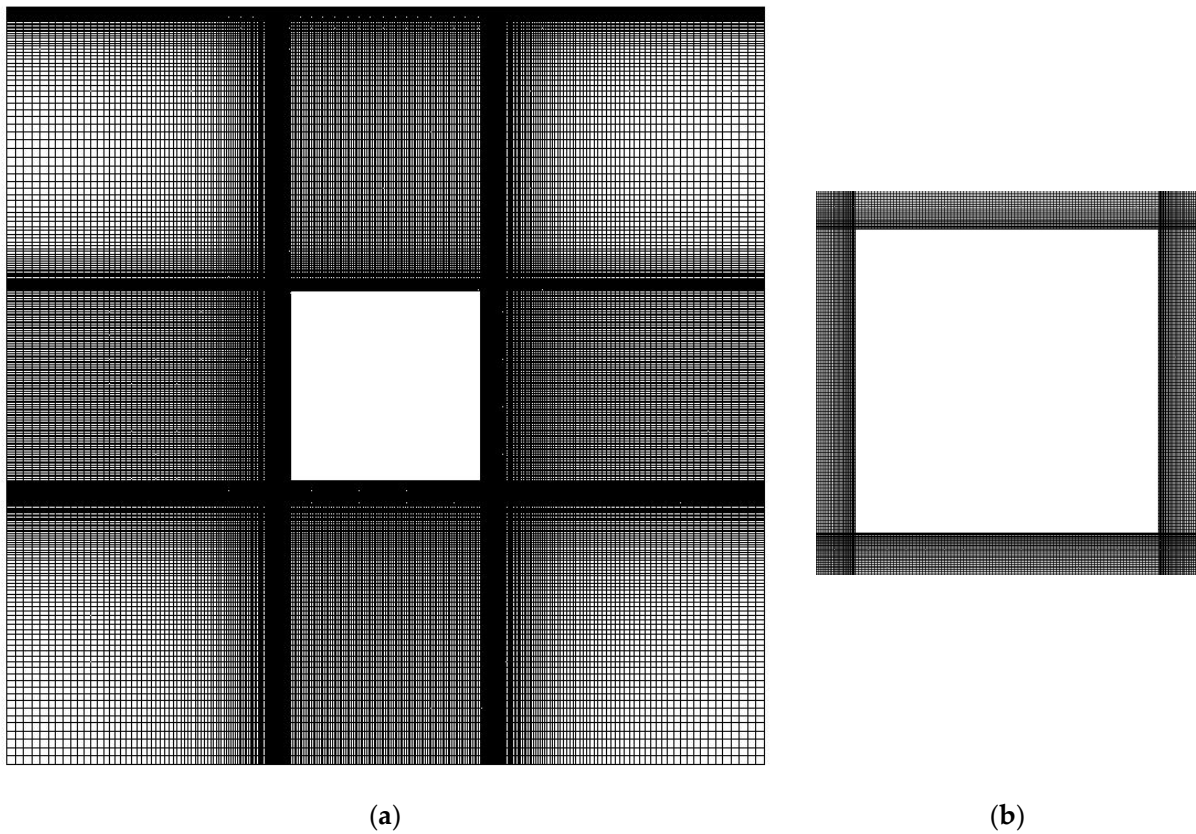


Figure 2. Computational grid; (a) Solution domain; (b) Grid in the vicinity of the square block.

Table 2. Grid convergence for $Ri = 0.1$ for pure water ($\phi = 0$).

Grid	Nodes	Nu_{avg}
150 × 150	20,400	7.416
225 × 225	45,600	7.393
255 × 255	58,480	7.383
285 × 285	72,960	7.378
300 × 300	80,800	7.376

2.5. Validation of Results

Table 3 presents the validation of the results. It compares the average Nusselt number values on the hot moving lid in a square lid-driven cavity for $Gr = 100$ and $Pr = 0.71$ with multiple studies. Furthermore, the numerical results are also compared for average Nusselt numbers on a concentric square blockage ($B = 1/4$) for $Ri = 0.1$ –10. Both Tables 3 and 4 indicate a strong agreement between the numerical results obtained from the present study and those of other studies.

Table 3. Comparison of average Nusselt number for $Gr = 100$ and $Pr = 0.71$.

Authors	Re		
	100	400	1000
Iwatsu et al. [6]	1.94	3.84	6.33
Astanina et al. [24]	2.05	4.09	6.70
Mehmood et al. [26]	2.03	4.07	6.58
Sivasankaran et al. [3]	-	4.09	6.48
Abu-Nada and Chamka [17]	2.09	4.16	6.55
Present Study	1.88	3.83	6.38

Table 4. Comparison of average Nusselt number for concentric square blockage with Islam et al. [11] and Mehmood et al. [26].

Ri	Islam et al. [11]	Mehmood et al. [26]	Present Study
0.1	5.6118	5.5317	5.5317
1	5.6935	5.5684	5.5755
10	7.9083	7.9029	7.9144

3. Results

The numerical calculations were conducted for a constant Grashof number (Gr) of 100. The Richardson number (Ri) was varied within the range of 0.01 to 100, while the nanofluid particle range (ϕ) was set from 0 to 0.05. The Richardson number is defined as the ratio of Grashof number to the square of the Reynolds number ($Ri = Gr/Re^2$).

Figure 3a,b illustrates the streamlines and isotherms for a range of Richardson numbers (Ri) from 0.01 to 100, considering a nanofluid with a volume fraction (ϕ) of 0.04. In all cases, a single clockwise cell is observed. The nanofluid located over the left upper corner is pulled upwards towards the top lid and circulates due to the shear force exerted by the moving top lid. For $Ri = 0.01$, a single cell appears over the right top corner of the blockage. As the Richardson number increases, the cells grow in size until $Ri = 10$, and the center of the cell moves over the blockage. At $Ri = 100$, the cell further expands. The rightward movement of the lid leads to the formation of steep velocity gradients near the top lid. Throughout all cases, there exists a gap between the blockage and the left-right and lower walls of the cavity. This gap tends to widen as the Richardson number increases. Consequently, as the Richardson number increases, there is minimal flow over the blockage surfaces. The isotherms provide insights into the influence of the Richardson number within the cavity. Temperature gradients are more pronounced near the blockage surfaces. For lower Richardson number values, the movement of the top lid affects the blockage, resulting in a temperature gradient over the left top corner of the blockage, which is observed up to $Ri = 1$. However, for $Ri = 10$ –100, the effect of natural convection becomes dominant over forced convection, and only a temperature gradient is observed around the blockage.

Figure 4a,b illustrates the velocity profiles for U-velocity and V-velocity along the horizontal and vertical midplane within the cavity. The U-velocity profiles exhibit similar characteristics, but the position of the bubble influences the U-velocity values. Between the blockage and the top lid, the U-velocity values initiate at the lid velocity, reach a minimum, and then increase to zero at the blockage surface. In the lower space between the blockage and the bottom wall of the cavity, the U-velocity values are negative due to the clockwise stream and remain nearly constant for all Richardson number values. On the other hand, the V-velocity values are positive due to the upward flow between the left wall and the blockage, and negative due to the downward flow between the right wall and the blockage. As the Richardson values increase, the maximum values of V-velocity and their corresponding positions tend to shift closer to the blockage. In the region between the right wall of the cavity and the blockage, the minimum values of V-velocity decrease with increasing Richardson number values, and the locations of these minimum V-velocity values tend to approach the right wall of the cavity.

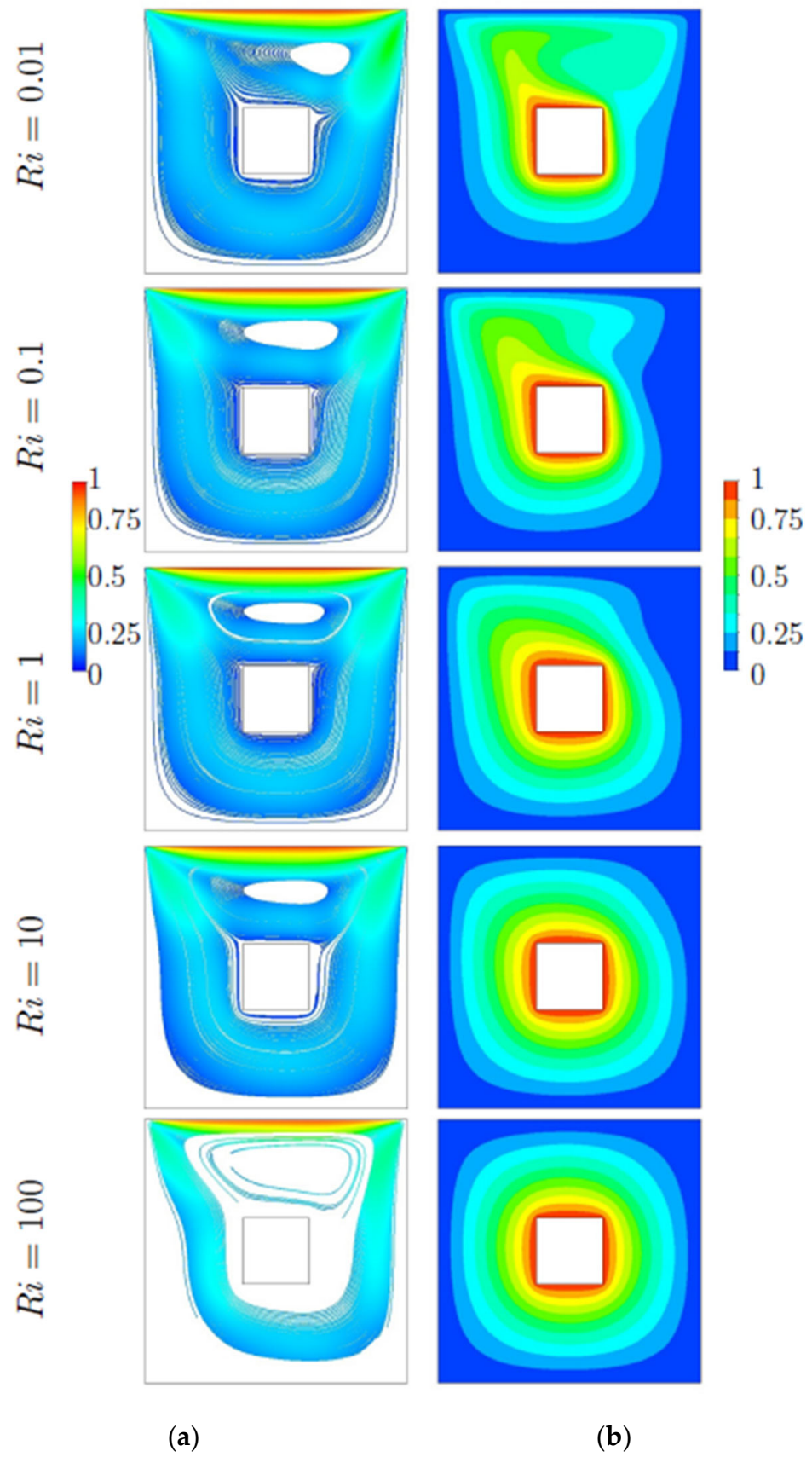


Figure 3. Streamlines (a) and isotherms (b) for $\phi = 0.04$.

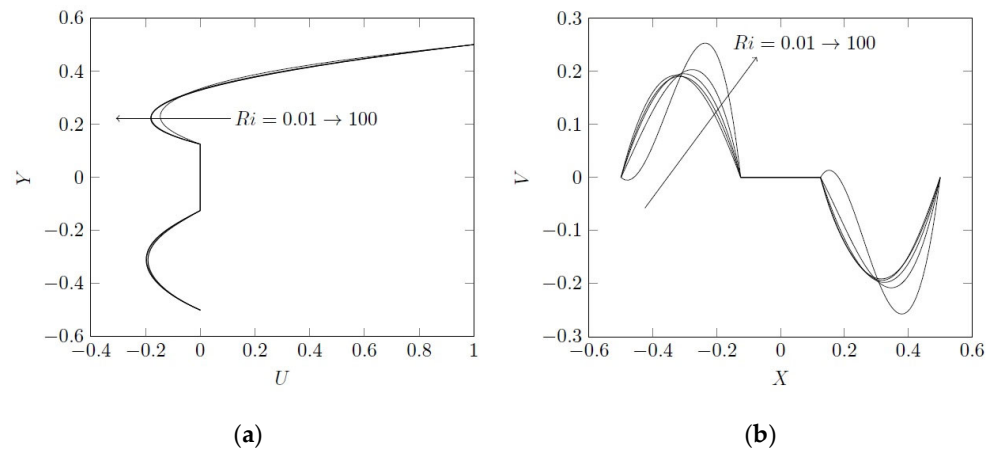


Figure 4. Velocity profiles at vertical (a) and horizontal (b) mid-plane.

In Figure 5a,b, the Nusselt number values for the square blockage surfaces are presented for the nanofluid volume fraction and Richardson numbers. It is observed that for $Ri = 0.01$ – 0.1 – 1 , the right surface exhibits the highest Nusselt number values, followed by the top, bottom, and left surfaces, respectively. On the other hand, for $Ri = 10$ – 100 , where the dominant heat transfer mode is natural convection, the highest Nusselt number values are obtained on the right surface of the blockage, followed by the bottom, top, and left surfaces. Furthermore, it is noted that the Nusselt number values decrease as the Richardson number increases and the nanofluid volume fraction decreases.

Table 5 displays the average Nusselt number values for the various surfaces, namely the right, bottom, left, and top surfaces. In Figure 5a,b, the Nusselt number values for the square blockage surfaces are presented, considering the nanofluid volume fraction and Richardson numbers. When $Ri = 0.01$ – 0.1 – 1 , it is observed that the right surface exhibits the highest Nusselt number values, followed by the top, bottom, and left surfaces, respectively. However, for $Ri = 10$ – 100 , where the dominant heat transfer mode is natural convection, the right surface of the blockage obtains the highest Nusselt number values, followed by the bottom, top, and left surfaces. It is worth noting that the Nusselt number values decrease as the Richardson number increases and the nanofluid volume fraction decreases.

Table 5. Average Nusselt number values of square blockage right, bottom, left, and top faces for Richardson number and nanofluid particle range values.

Nu_{avg}					
$\phi = 0.01$					
	$Ri = 0.01$	$Ri = 0.1$	$Ri = 1$	$Ri = 10$	$Ri = 100$
Right	14.14	10.51	7.27	5.76	5.37
Bottom	8.87	7.02	5.61	5.34	5.31
Left	6.74	5.37	4.71	4.89	5.09
Top	9.97	8.49	6.01	5.23	5.13
$\phi = 0.02$					
	$Ri = 0.01$	$Ri = 0.1$	$Ri = 1$	$Ri = 10$	$Ri = 100$
Right	14.44	10.71	7.40	5.90	5.51
Bottom	9.07	7.15	5.75	5.49	5.45
Left	6.89	5.47	4.84	5.03	5.23
Top	10.18	8.63	6.14	5.38	5.27

Table 5. Cont.

Nu_{avg}					
$\phi = 0.03$					
	$Ri = 0.01$	$Ri = 0.1$	$Ri = 1$	$Ri = 10$	$Ri = 100$
Right	14.76	10.92	7.54	6.04	5.66
Bottom	9.26	7.30	5.89	5.63	5.60
Left	7.04	5.58	4.97	5.18	5.39
Top	10.38	8.79	6.27	5.53	5.43
$\phi = 0.04$					
	$Ri = 0.01$	$Ri = 0.1$	$Ri = 1$	$Ri = 10$	$Ri = 100$
Right	15.08	11.13	7.68	6.18	5.80
Bottom	9.47	7.44	6.03	5.78	5.76
Left	7.19	5.70	5.11	5.33	5.53
Top	10.60	8.93	6.39	5.67	5.58
$\phi = 0.05$					
	$Ri = 0.01$	$Ri = 0.1$	$Ri = 1$	$Ri = 10$	$Ri = 100$
Right	15.39	11.34	7.82	6.34	5.96
Bottom	9.69	7.59	6.18	5.94	5.90
Left	7.35	5.82	5.24	5.48	5.69
Top	10.83	9.09	6.53	5.82	5.73

The average Nusselt number on square blockage for all cases examined in the study is presented in Table 6. Figure 6 provides a visual representation of how the average Nusselt number on the surface of square blockages varies with changes in the Richardson number and the volume fraction of the nanofluid. It is observed that as the Richardson number increases, there is a corresponding decrease in the average Nusselt number on the surface of square blockages. On the other hand, an increase in the nanofluid volume fraction increases the average Nusselt number on the surface of square blockages. Based on these findings, a relationship between the average Nusselt number, the Richardson number, and the nanofluid volume fraction is established. This relationship is valid within the range of $0.01 \leq Ri \leq 100$ and $0 \leq \phi \leq 0.05$.

$$Nu_{avg} = 6.3572Ri^{-0.0792}8.9695\phi \quad (r^2 = 0.926) \quad (18)$$

Table 6. Average Nusselt number values of square blockage for Richardson number and nanofluid particle range values.

Nu_{avg}						
Ri	$\phi=0$	$\phi=0.01$	$\phi=0.02$	$\phi=0.03$	$\phi=0.04$	$\phi=0.05$
0.01	9.52	9.73	9.94	10.15	10.37	10.59
0.1	7.54	7.68	7.83	7.98	8.13	8.28
1	5.68	5.80	5.93	6.06	6.19	6.33
10	5.10	5.24	5.38	5.52	5.67	5.82
100	5.02	5.15	5.31	5.45	5.60	5.76

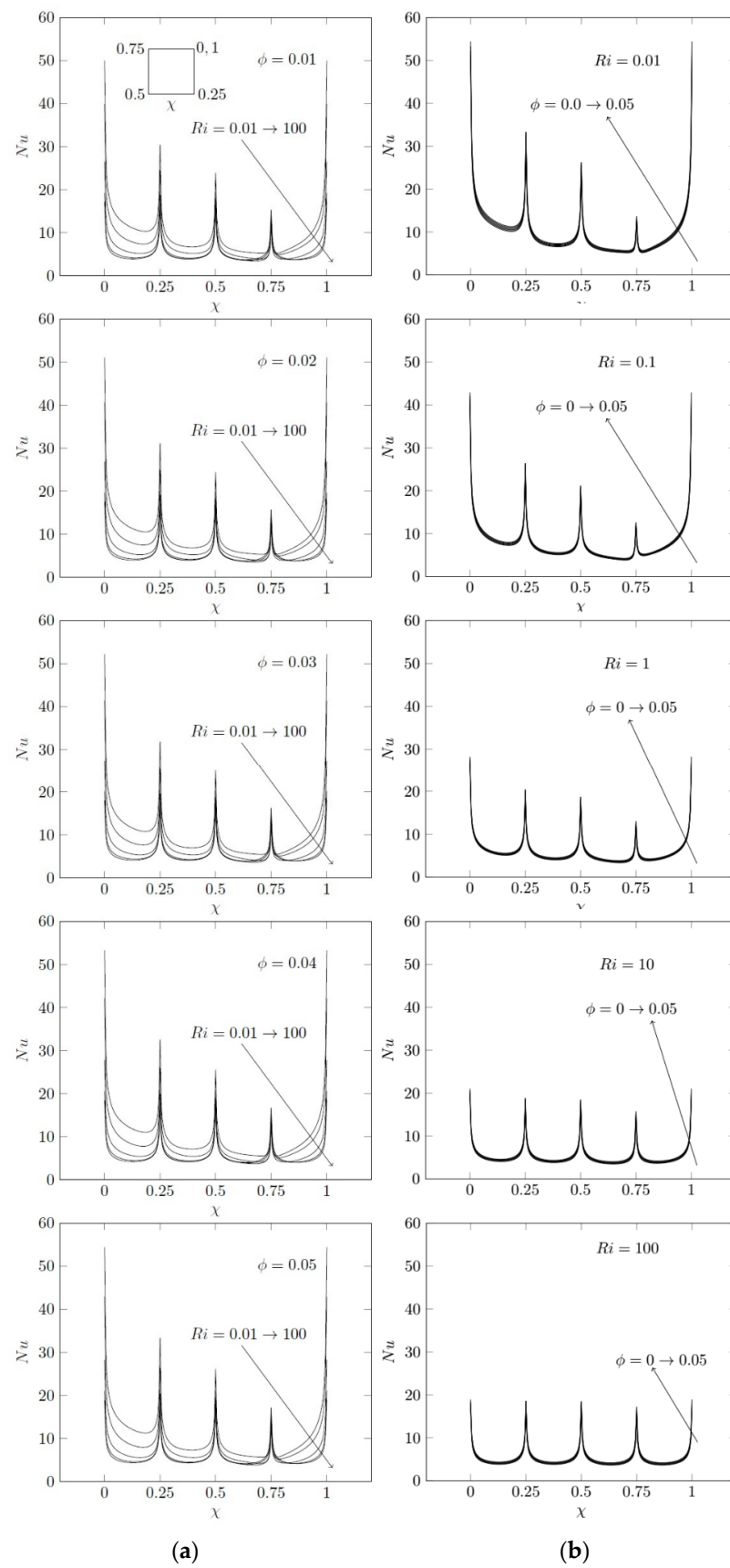


Figure 5. Nusselt number variation on blockage surfaces for $\phi = 0.01\text{--}0.05$ (a) and $Ri = 0.01\text{--}100$ (b).

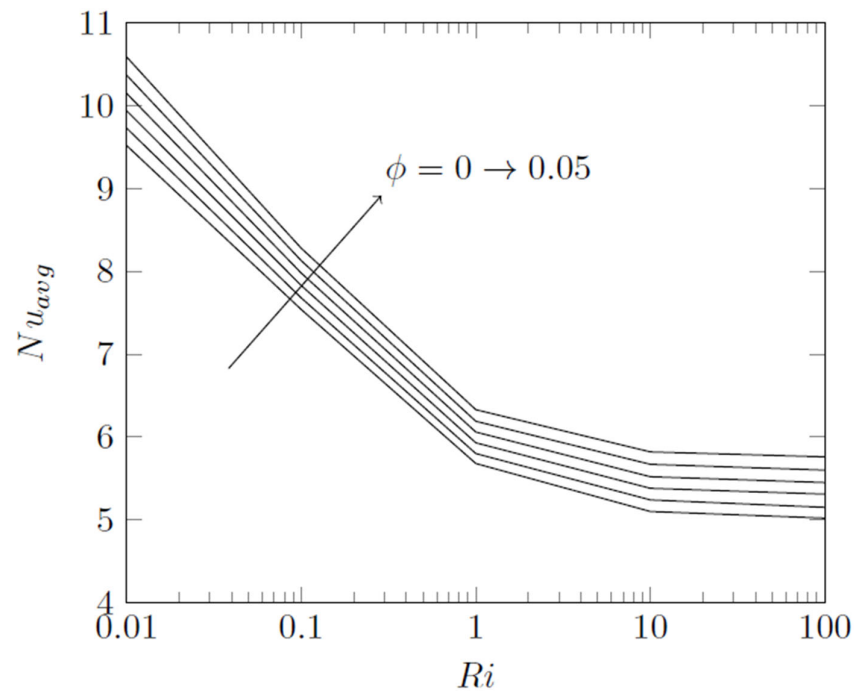


Figure 6. Average Nusselt number on blockage surface for $\phi = 0.01$ – 0.05 and $Ri = 0.01$ – 100 .

Table 7 presents the dimensionless total entropy generation of the system with the Richardson number and nanofluid particle fraction. The findings indicate that the dimensionless total entropy generation of the system increases as the nanofluid particle fraction increases. Conversely, the dimensionless entropy generation of the system increases as the Richardson numbers decrease, particularly when forced convection is dominant. As the Richardson numbers increase, natural convection takes over as the primary heat transfer mechanism. For Richardson numbers of $Ri = 10$ and $Ri = 100$, the changes in the dimensionless total entropy value are not significant due to the dominance of natural convection. The calculations demonstrate that heat transfer irreversibility plays a major role in the total entropy generation. Figure 7 illustrates the variation of total dimensionless entropy with the Richardson number and nanofluid volume fraction. It is evident from Figure 7 that the total dimensionless entropy values exhibit a sharp decrease until Richardson number values of $Ri = 1$, where the Reynolds number becomes dominant. Furthermore, Equation (15) provides a derived relationship for the total dimensionless entropy generation with the Richardson number and nanofluid volume fraction.

$$S_{total} = 14.62Ri^{-0.1131}115.5095\phi \quad (r^2 = 0.941) \quad (19)$$

Table 7. Dimensionless total entropy generation for Richardson number and nanofluid particle range values.

Ri	S_{total}					
	$\phi=0$	$\phi=0.01$	$\phi=0.02$	$\phi=0.03$	$\phi=0.04$	$\phi=0.05$
0.01	25.44	26.71	28.03	29.41	30.85	32.35
0.1	18.79	19.61	20.47	21.37	22.30	23.28
1	12.60	13.20	13.84	14.51	15.21	15.95
10	10.86	11.46	12.09	12.75	13.45	14.17
100	10.63	11.24	11.87	12.53	13.23	13.95

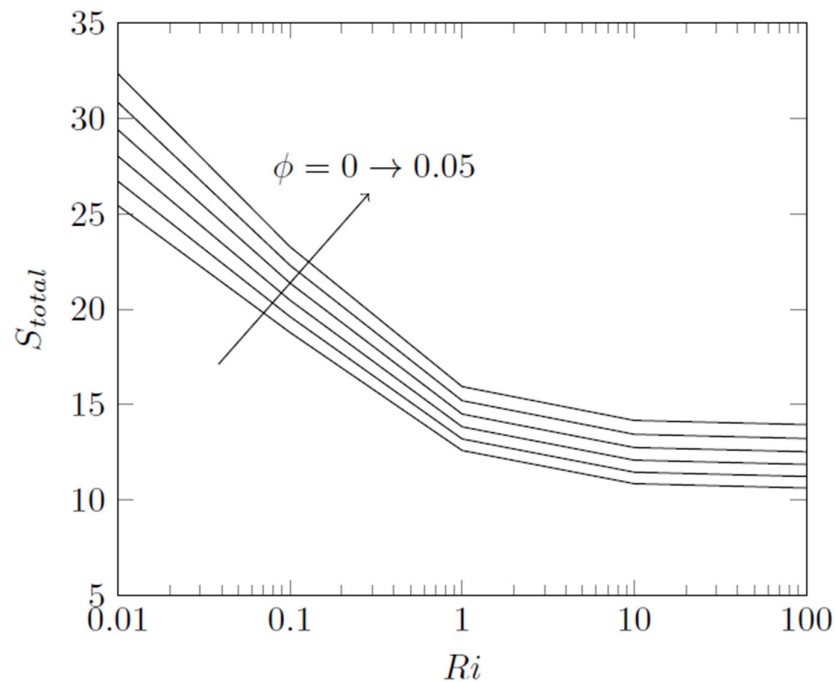


Figure 7. Total dimensionless entropy for $\phi = 0.01\text{--}0.05$ and $Ri = 0.01\text{--}100$.

4. Conclusions

The main objective of the numerical study is to examine the mixed convection occurring in a square cavity filled with a nanofluid consisting of Al_2O_3 particles and water. The cavity is being driven by a lid, and there is an isothermally heated square blockage positioned at the center of the cavity. The study investigates the heat transfer, flow characteristics, and the total dimensionless entropy of the flow. The influence of the Richardson number and the volume fraction of the nanofluid on heat transfer, the flow characteristics, and the total entropy generation of the nanofluid are investigated while maintaining a constant Grashof number of $Gr = 100$. Streamlines, isotherms, velocity profiles on the central plane of the cavity, variations in the Nusselt number on the square blockage surfaces, mean values of the Nusselt number on the square blockage surface, and the overall dimensionless entropy generation of the system are acquired. The following conclusions can be withdrawn from the study:

1. In each nanofluid volume fraction scenario, the dimensionless V-velocity remains constant on the horizontal midplane. However, the dimensionless V-velocity profile on this plane is influenced by the Richardson number. As the Richardson number increases, the maximum value of the dimensionless V-velocity also increases, and the position of this maximum value tends to shift toward the right. Nusselt number variations on the square blockage surfaces show that for $Ri = 0.01\text{--}0.1\text{--}1$, the highest Nusselt number values were obtained on the right surface, followed by top, bottom, and left surfaces, respectively. For $Ri = 10\text{--}100$, the highest Nusselt number values are calculated on the right surface but followed by the bottom, top, and left surfaces, respectively.
2. The dimensionless U-velocity values on the vertical midplane remain constant for every Richardson number and nanofluid volume fraction case. Similarly, the findings reveal that the velocity profile between the bottom wall of the square blockage and the bottom wall remains unchanged across all cases. However, a slightly different velocity profile is calculated between the top surface of the blockage and the top wall of the cavity in the $Ri = 0.01$ case, attributed to the positioning of the vortex cell.
3. The streamlines reveal that a singular vortex cell is obtained for every Richardson number instance. When $Ri = 0.01$, the cell is located above the top-right corner of the

square blockage, whereas for other Richardson number cases, the cell is positioned directly over the blockage. As the Richardson number increases, the gap between the bottom surface of the blockage and the bottom wall expands.

4. As the Richardson number rises, there is a decrease in temperature values between the top surface and the top wall. When $Ri = 100$, a uniform temperature distribution is achieved as the natural convection heat transfer mechanism dominates.
5. Increasing the volume fraction of the nanofluid and reducing the Richardson number leads to an increase in the average Nusselt number on the surface of the square blockage.
6. By considering the Richardson number and the volume fraction of the nanofluid, a correlation is derived for the average Nusselt number on the surface of a square blockage with a high degree of certainty ($r^2 = 0.926$).
7. The total dimensionless entropy of the flow shows an increase as the Richardson number decreases and the volume fraction of the nanofluid increases.
8. A correlation is established between the total dimensionless entropy and the variations in the Richardson number and the volume fraction of the nanofluid with a regression coefficient of $r^2 = 0.941$.

In future studies, different cavity shapes, different nanofluid types, and optimization of blockage shapes and dimensions for enhancing heat transfer and minimizing the entropy generation are planned.

Funding: This research received no external funding.

Data Availability Statement: Data are contained within the article.

Conflicts of Interest: The author declares no conflicts of interest.

Nomenclature

h	Hot
B	Blockage ratio
c	Cold
C_p	Specific heat at constant pressure (kJ/kgK)
f	Fluid
g	Gravitational acceleration (m/s ²)
Gr	Grashof number
H	Height of the cavity (m)
k	Thermal conductivity (W/mK)
L	Length of the cavity (m)
nf	Nanofluid
Nu	Nusselt number
p	Dimensional pressure (Pa)
P	Dimensionless pressure
Pr	Prandtl number
Re	Reynolds number
Ri	Richardson number
s	Local entropy (W/m ³ K)
sp	Solid particle
S	Dimensionless Entropy
T	Dimensional temperature (K)
u, v	Dimensional x and y velocity components (m/s)
U, V	Dimensionless x and y velocity
U_{lid}	Lid velocity (m/s)

x, y	Dimensional coordinates (m)
X, Y	Dimensionless coordinates
Greek Symbols	
α	Thermal diffusivity (m^2/s)
β	Thermal expansion coefficient ($1/\text{K}$)
ϕ	Nanoparticle volume fraction
ν	Kinematic viscosity (m^2/s)
θ	Dimensionless temperature
ρ	Density (kg/m^3)
μ	Dynamic viscosity (Pa s)

References

1. Erturk, E. Discussions on driven cavity flow. *Int. J. Numer. Methods Fluids* **2009**, *60*, 275–294. [[CrossRef](#)]
2. Ghia, U.; Ghia, K.; Shin, C. High-Re solutions for incompressible flow using the Navier-Stokes equations and a multigrid method. *J. Comput. Phys.* **1982**, *48*, 387–411. [[CrossRef](#)]
3. Sivasankaran, S.; Sivakumar, V.; Hussein, A.K.; Prakash, P. Mixed convection in a lid-driven two-dimensional square cavity with corner heating and internal heat generation. *Numer. Heat Transf. Part A Appl.* **2014**, *65*, 269–286. [[CrossRef](#)]
4. Azizul, F.M.; Alsabery, A.; Hashim, I. Heatlines visualisation of mixed convection flow in a wavy heated cavity filled with nanofluids and having an inner solid block. *Int. J. Mech. Sci.* **2020**, *175*, 105529. [[CrossRef](#)]
5. Jumadi, A.; Arbin, N.; Saleh, H.; Kechil, S.A. A Review of Entropy Generation in Rectangular Cavities. *J. Adv. Res. Fluid Mech. Therm. Sci.* **2024**, *115*, 178–221. [[CrossRef](#)]
6. Iwatsu, R.; Hyun, J.M.; Kuwahara, K. Mixed convection in a driven cavity with a stable vertical temperature gradient. *Int. J. Heat Mass Transf.* **1993**, *36*, 1601–1608. [[CrossRef](#)]
7. Malleswaran, A.; Sivasankaran, S. A Numerical Simulation on MHD Mixed Convection in a Lid-driven Cavity with Corner Heaters. *J. Appl. Fluid Mech.* **2016**, *9*, 311–319. [[CrossRef](#)]
8. Oztop, H.F.; Zhao, Z.; Yu, B. Fluid flow due to combined convection in lid-driven enclosure having a circular body. *Int. J. Heat Fluid Flow* **2009**, *30*, 886–901. [[CrossRef](#)]
9. Khanafer, K.; Aithal, S. Laminar mixed convection flow and heat transfer characteristics in a lid driven cavity with a circular cylinder. *Int. J. Heat Mass Transf.* **2013**, *66*, 200–209. [[CrossRef](#)]
10. Zheng, G.F.; Ha, M.Y.; Yoon, H.S.; Park, Y.G. A numerical study on mixed convection in a lid-driven cavity with a circular cylinder. *J. Mech. Sci. Technol.* **2013**, *27*, 273–286. [[CrossRef](#)]
11. Islam, A.W.; Sharif, M.A.; Carlson, E.S. Mixed convection in a lid driven square cavity with an isothermally heated square blockage inside. *Int. J. Heat Mass Transf.* **2012**, *55*, 5244–5255. [[CrossRef](#)]
12. Morshed, K.N.; Sharif, M.A.R.; Islam, A.W. Laminar Mixed Convection in a Lid-Driven Square Cavity with Two Isothermally Heated Square Internal Blockages. *Chem. Eng. Commun.* **2015**, *202*, 1176–1190. [[CrossRef](#)]
13. Gangawane, K.M. Computational analysis of mixed convection heat transfer characteristics in lid-driven cavity containing triangular block with constant heat flux: Effect of Prandtl and Grashof numbers. *Int. J. Heat Mass Transf.* **2017**, *105*, 34–57. [[CrossRef](#)]
14. Choi, S.U.S.; Eastman, J.A. Enhancing thermal conductivity of fluids with nanoparticles. *Am. Soc. Mech. Eng.* **1995**, *66*, 99–105. [[CrossRef](#)]
15. Xuan, Y.; Li, Q. Heat transfer enhancement of nano fluids. *Heat Fluid Flow* **2000**, *21*, 58–64. [[CrossRef](#)]
16. Khanafer, K.; Vafai, K.; Lightstone, M. Buoyancy-driven heat transfer enhancement in a two-dimensional enclosure utilizing nanofluids. *Int. J. Heat Mass Transf.* **2003**, *46*, 3639–3653. [[CrossRef](#)]
17. Abu-Nada, E.; Chamkha, A.J. Mixed convection flow in a lid-driven inclined square enclosure filled with a nanofluid. *Eur. J. Mech. B/Fluids* **2010**, *29*, 472–482. [[CrossRef](#)]
18. Mansour, M.; Mohamed, R.; Abd-Elaziz, M.; Ahmed, S.E. Numerical simulation of mixed convection flows in a square lid-driven cavity partially heated from below using nano fluid. *Int. Commun. Heat Mass Transf.* **2010**, *37*, 1504–1512. [[CrossRef](#)]
19. Talebi, F.; Mahmoudi, A.H.; Shahi, M. Numerical study of mixed convection flows in a square lid-driven cavity utilizing nano fluid. *Int. Commun. Heat Mass Transf.* **2010**, *37*, 79–90. [[CrossRef](#)]
20. Chamkha, A.J.; Abu-Nada, E. Mixed convection flow in single- and double-lid driven square cavities filled with water— Al_2O_3 nanofluid: Effect of viscosity models. *Eur. J. Mech. B/Fluids* **2012**, *36*, 82–96. [[CrossRef](#)]
21. Mojumder, S.; Saha, S.; Saha, S.; Mamun, M.A.H. Combined effect of Reynolds and Grashof numbers on mixed convection in a lid-driven T-shaped cavity filled with water- Al_2O_3 nanofluid. *J. Hydrodyn.* **2015**, *27*, 782–794. [[CrossRef](#)]
22. Kareem, A.K.; Mohammed, H.; Hussein, A.K.; Gao, S. Numerical investigation of mixed convection heat transfer of nano fluids in a lid-driven trapezoidal cavity. *Int. Commun. Heat Mass Transf.* **2016**, *77*, 195–205. [[CrossRef](#)]
23. Taamneh, Y.; Bataineh, K. Mixed Convection Heat Transfer in a Square Lid-Driven Cavity Filled with Al_2O_3 -Water Nanofluid. *Stroj. Vestn.-J. Mech. Eng.* **2017**, *63*, 383–393. [[CrossRef](#)]

24. Astanina, M.S.; Sheremet, M.A.; Oztop, H.F.; Abu-Hamdeh, N. Mixed convection of Al₂O₃-water nanofluid in a lid-driven cavity having two porous layers. *Int. J. Heat Mass Transf.* **2018**, *118*, 527–537. [[CrossRef](#)]
25. Cho, C. Heat transfer and entropy generation of mixed convection flow in Cu-water nanofluid-filled lid-driven cavity with wavy surface. *Int. J. Heat Mass Transf.* **2018**, *119*, 163–174. [[CrossRef](#)]
26. Mehmood, K.; Hussain, S.; Sagheer, M. Mixed convection in alumina-water nanofluid filled lid-driven square cavity with an isothermally heated square blockage inside with magnetic field effect: Introduction. *Int. J. Heat Mass Transf.* **2017**, *109*, 397–409. [[CrossRef](#)]
27. Karbasifar, B.; Akbari, M.; Toghraie, D. Mixed convection of Water-Aluminum oxide nanofluid in an inclined lid-driven cavity containing a hot elliptical centric cylinder. *Int. J. Heat Mass Transf.* **2018**, *116*, 1237–1249. [[CrossRef](#)]
28. Rajesh, V.; Sheremet, M. Free Convection in a Square Ternary Hybrid Nanoliquid Chamber with Linearly Heating Adjacent Walls. *Nanomaterials* **2023**, *13*, 2860. [[CrossRef](#)]
29. Bao, J.; Heyd, R.; Régnier, G.; Ammar, A.; Peixinho, J. Viscosity of graphene in lubricating oil, ethylene glycol and glycerol. *J. Therm. Anal. Calorim.* **2023**, *148*, 11455–11465. [[CrossRef](#)]
30. Chamkha, A.J.; Selimefendigil, F.; Oztop, H.F. MHD mixed convection and entropy generation in a lid-driven triangular cavity for various electrical conductivity models. *Entropy* **2018**, *20*, 903. [[CrossRef](#)]
31. Alshare, A.; Abderrahmane, A.; Guedri, K.; Younis, O.; Fayz-Al-Asad, M.; Ali, H.M.; Al-Kouz, W. Hydrothermal and Entropy Investigation of Nanofluid Natural Convection in a Lid-Driven Cavity Concentric with an Elliptical Cavity with a Wavy Boundary Heated from Below. *Nanomaterials* **2022**, *12*, 1392. [[CrossRef](#)]
32. Ishak, M.S.; Alsabery, A.I.; Hashim, I.; Chamkha, A.J. Entropy production and mixed convection within trapezoidal cavity having nanofluids and localised solid cylinder. *Sci. Rep.* **2021**, *11*, 14700. [[CrossRef](#)]
33. Laidoudi, H.; Abderrahmane, A.; Saeed, A.M.; Guedri, K.; Younis, O.; Marzouki, R.; Chung, J.D.; Shah, N.A. Lid-Driven Chamber with 3D Elliptical Obstacle under the Impacts of the Nano-Properties of the Fluid, Lorentz Force, Thermal Buoyancy, and Space Porosity. *Nanomaterials* **2022**, *12*, 2373. [[CrossRef](#)] [[PubMed](#)]
34. Maneengam, A.; Laidoudi, H.; Abderrahmane, A.; Rasool, G.; Guedri, K.; Weera, W.; Younis, O.; Bouallegue, B. Entropy Generation in 2D Lid-Driven Porous Container with the Presence of Obstacles of Different Shapes and under the Influences of Buoyancy and Lorentz Forces. *Nanomaterials* **2022**, *12*, 2206. [[CrossRef](#)] [[PubMed](#)]
35. Maneengam, A.; Bouzennada, T.; Abderrahmane, A.; Guedri, K.; Weera, W.; Younis, O.; Bouallegue, B. Numerical Study of Lid-Driven Hybrid Nanofluid Flow in a Corrugated Porous Cavity in the Presence of Magnetic Field. *Nanomaterials* **2022**, *12*, 2390. [[CrossRef](#)]
36. Taghizadeh, S.; Asaditaheri, A. Heat transfer and entropy generation of laminar mixed convection in an inclined lid driven enclosure with a circular porous cylinder. *Int. J. Therm. Sci.* **2018**, *134*, 242–257. [[CrossRef](#)]
37. Zeghibid, I.; Bessaïh, R. Mixed convection and entropy generation in a square cavity using nanofluids. *Thermophys. Aeromechanics* **2018**, *25*, 245–256. [[CrossRef](#)]
38. Garnett, J.C.M. Colours in metal glasses and in metallic films. *Philos. Trans. R. Soc. Ser. A* **1904**, *203*, 385–420. [[CrossRef](#)]
39. Brinkman, H.C. The viscosity of concentrated suspensions and solutions. *J. Chem. Phys.* **1952**, *20*, 571–581. [[CrossRef](#)]

Disclaimer/Publisher’s Note: The statements, opinions and data contained in all publications are solely those of the individual author(s) and contributor(s) and not of MDPI and/or the editor(s). MDPI and/or the editor(s) disclaim responsibility for any injury to people or property resulting from any ideas, methods, instructions or products referred to in the content.